apparent k_{cat}. Thus, the efficiency of ATP hydrolysis during unwinding can easily be calculated from the data used to define the helicase and ATPase units.

ACKNOWLEDGMENTS

We are grateful to Andrew Taylor, Dennis Schultz, and Gerald Smith of the Fred Hutchinson Cancer Center in Seattle for the gift of *E. coli* strains and recBCD enzyme with which preliminary experiments were performed. We are also grateful to Joseph P. Menetski for critical reading of the manuscript.

Registry No. ATPase, 9000-83-3; ATP, 56-65-5; magnesium, 7439-95-4.

REFERENCES

Eichler, D. C., & Lehman, I. R. (1977) *J. Biol. Chem. 252*, 499–503.

Finch, P. W., Storey, A., Chapman, K. E., Brown, K., Hickson, I. D., & Emmerson, P. T. (1986a) *Nucleic Acids Res. 21*, 8573–8582.

Finch, P. W., Wilson, R. E., Brown, K., Hickson, I. D., Tomkinson, A. E., & Emmerson, P. T. (1986b) *Nucleic Acids Res. 11*, 4437–4451.

Finch, P. W., Storey, A., Brown, K., Hickson, I. D., & Emmerson, P. T. (1986c) *Nucleic Acids Res. 21*, 8583–8594.

Goldmark, P. J., & Linn, S. (1972) *J. Biol. Chem. 247*, 1849–1860.

Hickson, I. D., Atkinson, K. E., Hutton, L., Tomkinson, A. E., & Emmerson, P. T. (1984) *Nucleic Acids Res. 12*, 3807–3819.

Hickson, I. D., Robson, C. N., Atkinson, K. E., Hutton, L., & Emmerson, P. T. (1985) *J. Biol. Chem. 260*, 1224–1229.

Julin, D. A., & Lehman, I. R. (1987) *J. Biol. Chem. 262*, 9044–9051.

Karu, A. E., & Linn, S. (1972) *Proc. Natl. Acad. Sci. U.S.A. 69*, 2855–2859.

Karu, A. E., MacKay, V., Goldmark, P. J., & Linn, S. (1973) *J. Biol. Chem. 248*, 4874–4884.

Kreuzer, K. N., & Jongeneel, C. V. (1983) *Methods Enzymol. 100*, 144–160.

Lieberman, H. B., & Oishi, M. (1974) *Proc. Natl. Acad. Sci. U.S.A. 71*, 4816–4820.

MacKay, V., & Linn, S. (1976) *J. Biol. Chem. 251*, 3716–3719.

Roman, L. J., & Kowalczykowski, S. C. (1989) *Biochemistry* (preceding paper in this issue).

Rosamond, J., Telander, K. M., & Linn, S. (1979) *J. Biol. Chem. 254*, 8646–8652.

Schultz, D. W., Taylor, A. F., & Smith, G. R. (1983) *J. Bacteriol. 155*, 664–680.

Taylor, A. F. (1988) *Genetic Recombination* (Kucherlapati, R., & Smith, G. R., Eds.) pp 231–263, American Society for Microbiology, Washington, DC.

Taylor, A. F., & Smith, G. R. (1980) *Cell (Cambridge, Mass.) 22*, 447–457.

Taylor, A. F., & Smith, G. R. (1985) *J. Mol. Biol. 185*, 431–443.

Taylor, A. F., Schultz, D. W., Ponticelli, A. S., & Smith, G. R. (1985) *Cell (Cambridge, Mass.) 41*, 153–163.

Telander-Muskavitch, K., & Linn, S. (1982) *J. Biol. Chem. 257*, 2641–2648.

Walker, J. E., Saraste, M., Runswick, M. J., & Gay, N. J. (1982) *EMBO J. 1*, 645–951.

Solution Structure of the Glycosylphosphatidylinositol Membrane Anchor Glycan of *Trypanosoma brucei* Variant Surface Glycoprotein†

S. W. Homans,‡ C. J. Edge, M. A. J. Ferguson,‡ R. A. Dwek,* and T. W. Rademacher

Oxford Glycobiology Unit, Department of Biochemistry, Oxford University, South Parks Road, Oxford OX1 3QU, England

Received August 8, 1988; Revised Manuscript Received November 18, 1988

ABSTRACT: The average solution conformation of the glycosylphosphatidylinositol (GPI) membrane anchor of *Trypanosoma brucei* variant surface glycoprotein (VSG) has been determined by using a combination of two-dimensional ^1H–^1H NMR methods together with molecular orbital calculations and restrained molecular dynamics simulations. This allows the generation of a model to describe the orientation of the glycan with respect to the membrane. This shows that the glycan exists in an extended configuration along the plane of the membrane and spans an area of 600 Å^2, which is similar to the cross-sectional area of a monomeric N-terminal VSG domain. Taken together, these observations suggest a possible space-filling role for the GPI anchor that may maintain the integrity of the VSG coat. The potential importance of the GPI glycan as a chemotherapeutic target is discussed in light of these observations.

The parasitic protozoan *Trypanosoma brucei* undergoes a complex life cycle between an insect (tsetse fly) vector and its mammalian hosts. *T. brucei* is the causative agent of ngana in cattle and is closely related to *Trypanosoma rhodesiense* and *Trypanosoma gambiense*, which cause human sleeping sickness. The parasite lives in the blood and lymph of the mammalian host where it is protected from lytic serum components by a dense monolayer of variant surface glycoprotein (VSG)[1] that forms a continuous macromolecular diffusion

† This work is a contribution from the Oxford Glycobiology Unit which is supported by Monsanto.

‡ Present address: Department of Biochemistry, Medical Sciences Institute, University of Dundee, Dundee, Scotland DD1 4HN.

[1] Abbreviations: GPI, glycosylphosphatidylinositol; VSG, variant surface glycoprotein; COSY, homonuclear correlated spectroscopy; NOESY, homonuclear nuclear Overhauser effect spectroscopy; NMR, nuclear magnetic resonance; MO, molecular orbital; MM, molecular mechanics; MD, molecular dynamics.

0006-2960/89/0428-2881$01.50/0

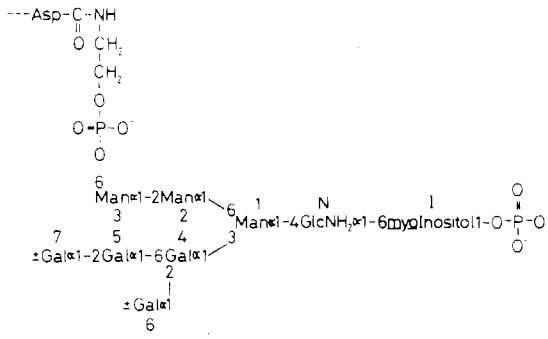

FIGURE 1: Structure of the GPI glycan of *T. brucei* investigated in this study.

barrier (Cross, 1974; Turner, 1985). Although a single trypanosome expresses only one VSG at a time, it contains several hundred genes encoding immunologically distinct VSG variants. A trypanosome population evades the host's humoral immune response by a small proportion of the cells undergoing antigenic variation to express new VSG genes. In this way the original population is destroyed by host antibody and is replaced by a new group of variants (Boothroyd, 1985; Van der Ploeg, 1987).

The VSGs of African trypanosomes are anchored to the plasma membrane via covalent linkage of the C-terminal amino acids to glycosylphosphatidylinositol (GPI) moieties, rather than via transmembrane hydrophobic polypeptide sequences. The GPI mechanism of membrane anchorage has been found throughout most stages of eukaryotic evolution and has been recently reviewed (Low & Saltiel, 1988; Ferguson & Williams, 1988).

Each VSG is composed of conformationally independent N-terminal and C-terminal domains, and three distinct VSG subgroups can be defined on the basis of polypeptide homology in the latter (Boothroyd, 1985). While structural data are available with regard to the N-terminal domains of VSGs (Metcalf et al., 1987), as yet no data are available regarding the three-dimensional structures of the C-terminal domains or the conformation of the associated GPI anchor. The complete three-dimensional structure is potentially of great interest, since each VSG variant is required to be immunologically distinct, and yet paradoxically all must presumably occupy similar volumes in order to maintain the integrity of the coat as a macromolecular diffusion barrier.

Recently, the complete chemical structure of the GPI glycan moiety of VSG MITat 1.4 variant 117 has been determined by using a combination of high-resolution proton NMR, mass spectrometry, and chemical and enzymatic degradation (Ferguson et al., 1988) (Figure 1). The highly branched nature of this glycan suggests a possible space-filling role that may maintain the integrity of the coat irrespective of the precise three-dimensional structure of each VSG variant.

Here, using a combination of two-dimensional ^1H–^1H NMR together with molecular orbital calculations and restrained molecular dynamics simulations, we describe the average solution conformation of the GPI glycan of MITat 1.4. These data allow the generation of a model that describes the orientation of the glycan with respect to the membrane.

Experimental Procedures

Sample Preparation. The soluble C-terminal glycopeptide (sCtgp) of VSG MITat 1.4 was isolated as described previously (Ferguson et al., 1988). This material contains the entire GPI structure, minus the *sn*-1,2-dimyristylglycerol lipid group, linked to the C-terminal aspartic acid residue of the VSG polypeptide. The sample was prepared for NMR analysis by repetitive dissolution in 99.96% D_2O (Aldrich) with intermediate flash evaporation and was finally dissolved in 400 μL of 99.96% D_2O to a concentration of ca. 500 μM.

NMR Studies. Homonuclear ^1H COSY and ^1H NOESY (Ernst et al., 1987) spectra were recorded as described previously (Ferguson et al., 1988). A mixing time of 300 ms was used in NOESY spectra, which ensured that all cross-peak intensities were measured within the initial rate approximation (Homans et al., 1987a). Cross-peak volumes were used in the generation of approximate interresidue distance constraints using intraresidue NOEs as reference distances and assuming overall isotropic motion (Homans et al., 1987a). Assignments of intraresidue and interresidue NOE connectivities to specific protons were obtained from COSY spectra, and these assignments have been described previously (Ferguson et al., 1988).

Molecular Orbital (MO) Calculations. These were computed by using the AMPAC molecular orbital package (Dewar & Stewart, 1986). All calculations were performed in vacuo. Potential surfaces for disaccharide fragments were obtained from a grid search about each glycosidic torsion angle ϕ and ψ, where ϕ = H1–C1–O1–CX, ψ = C1–O1–CX–HX, and HX and CX are aglyconic atoms. In the case of 1–6 glycosidic linkages, ψ = C1–O1–C6–C5 and ω = O6–C6–C5–H5.

Molecular Mechanics (MM) Calculations and Molecular Dynamics (MD) Simulations. These were computed by using AMBER (Weiner et al., 1986). For this purpose the original force field was reparametrized for oligosaccharides according to the procedure of Hopfinger and Pearlstein (1984) modified by inclusion of a nonlinear least-squares algorithm. This reparametrization consisted of recalculation of the potential barrier and phase terms of the relevant torsional parameters for each glycosidic linkage type, using molecular orbital (AMPAC) calculations as a basis. This reparametrization was found to be necessary since the original force field is parametrized only for peptides and nucleic acids, and the potential surfaces about glycosidic linkages obtained from the MM procedures using the original force field on disaccharides were significantly different from those obtained with MO calculations under the same conditions.

The MM and MD calculations were performed in vacuo. The effects of solvent in MM and MD calculations on the complete glycan were simulated in part by the inclusion of a large (ϵ = 50) dielectric constant into Coulombic terms of the force field. Approximate NOE distance constraints were included as harmonic restraints with a relatively weak force constant (5 kcal mol^{-1} Å^{-2}). Simulations of MD trajectories were computed by using the same force-field parametrization as MM calculations and proceeded in two parts. The molecule was coupled to a thermal bath with a relaxation time of 0.4 ps, and the temperature was slowly raised over a period of 3 ps from 10 to 300 K. After this equilibration period, dynamics trajectories were calculated over 3 ps under the same conditions at a constant temperature of 300 K. Coordinates were stored at intervals of 0.01 ps, and these were used to compute structures in Cartesian space over the course of the second 3 ps of the simulation.

Theoretical Solution Conformation. (a) Background to Method. The use of quantitative ^1H–H NOE measurements together with conformational energy calculations is a well-established method for the determination of solution conformations of N-linked glycoprotein glycans as "static" structures (Brisson & Carver, 1983a,b; Paulsen et al., 1984, 1986a,b; Homans et al., 1987a,b). However, more recent studies have

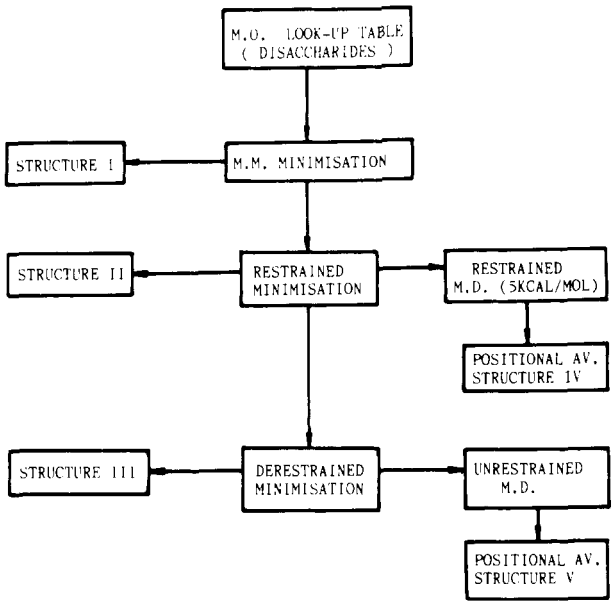

FIGURE 2: Strategy for the derivation of the three-dimensional average solution structure of the GPI glycan. For details see text.

addressed the question of oligosaccharide dynamics (Homans et al., 1987c; Cumming & Carver, 1987), and from these it is now clear that the orientation of two glycosidically linked monosaccharide residues may undergo torsional oscillations about the global minimum. In the majority of linkage types, these fluctuations are restricted to narrow torsional oscillations within a single, deep potential well, and the "average" conformation is closely approximated by the global minimum configuration (Homans et al., 1987c). However, in the case of α1–6 and β1–6 glycosidic linkages, these torsional oscillations are large due both to an extra degree of freedom and to greater mobility about glycosidic torsion angles (Homans et al., 1987c). The interpretation of NOE constraints in terms of a single fixed conformation about α1–6 and β1–6 glycosidic linkages may thus give a completely false picture of the preferred orientation due to r^{-6} weighting of internuclear distances. Correspondingly, the NOE-defined conformation often does not relate to the global minimum. In these cases we can only refer to an average conformation in Cartesian space about the glycosidic linkages.

In the present study, the determination of the solution conformation of the GPI glycan is complicated by the fact that the number of NOE constraints is less than the number of degrees of freedom defined by the torsional angles ϕ and ψ about each glycosidic linkage, and about the additional torsional angle ω in the case of α1–6 linkages. While conformational preferences about the latter can be assessed by measurement of spin coupling constants ($J_{5,6}$ and $J_{5,6'}$), the three-dimensional structure is still experimentally underdefined. In addition, since in some cases only one NOE is measurable across glycosidic linkages, the possibility of large torsional oscillations cannot a priori be ruled out. The approach that we have adopted in the present study for the determination of the solution conformation of the GPI glycan therefore differs from methods previously described (Homans et al., 1986, 1987a–c).

(*b*) *Procedure for GPI Glycan.* The procedure is outlined in Figure 2. Each glycosidic linkage is oriented into a global minimum configuration computed with semiempirical quantum mechanical (MO) calculations upon the relevant disaccharide fragments of which the glycan is composed. Such calculations, in principle, give a more accurate representation of the potential surface than those based on empirical functions, but are restricted to disaccharides and trisaccharides in view of their large computational requirements. The overall purpose of this stage is to orient the molecule into a conformation that lies close to the global minimum. The internal energy of this structure is then minimized to locate a more accurate global minimum for the intact molecule (structure I). This minimization is achieved by use of MM procedures, with a force field that is parametrized for oligosaccharides by using MO calculations (see above). This is followed by restrained minimization using approximate internuclear distances derived from NOE measurements to generate structure II. The associated force constants for these contraints are chosen to be relatively weak (5 kcal mol^{-1} A^{-2}) to reflect the possibility of motional averaging with consequent large errors in NOE distance constraints. The geometry of the molecule is then relaxed by reminimization with constraints removed. Accordingly, we refer to this structure as the derestrained minimized structure (III). Structures I, II, and III thus represent respectively the theoretical global minimum energy geometry for the complete structure, the geometry with NOE constraints imposed, and the new geometry corresponding to the global minimum obtained after inclusion of NOE constraints. Each of these structures is static and represents the conformation at 0 K. At 300 K, thermal motions are present, and it is therefore important to consider the implications of motional averaging within the molecule, particularly about glycosidic torsional angles as discussed above. Unfortunately, the magnitudes of NOEs across glycosidic linkages are rather poor parameters by which motional averages may be assessed in view of their nonlinear dependence upon internuclear distances. In previous studies, we have found molecular dynamics simulations to be useful in assessing the extent of conformational averaging in simple disaccharide models (Homans et al., 1987c). In the present study a similar approach was adopted for the complete glycan. For each of structures II and III, MD simulations were calculated at 300 K (see above) from which average structures in Cartesian space (structures IV and V) were calculated over the course of the simulation. Since the MM force field has been parametrized by using an MO basis, the simulation effectively represents thermal motions within the potential well(s) defined by the latter, with or without NOE constraints. Root mean square fluctuations of atomic positions are an indication of the relative mobilities of regions of the molecule.

Recently, a related procedure for the assessment of conformational averaging about glycosidic linkages has been described (Cumming & Carver, 1987). This is based upon a statistical mechanical analysis in order to determine the relative occupancy of discrete microstates on the potential surface at 300 K, from which theoretical NOEs can be calculated and compared with those determined experimentally. The present method differs in that the potential surface is calculated by using a parametrization based upon molecular orbital methods rather than an empirical hard-sphere potential, and the free dynamics simulations described here allow for motion about all degrees of freedom rather than being restricted to motion about ϕ and ψ for each linkage, which represents a small subset of the total conformational space.

RESULTS

The values of ϕ, ψ, and ω about each linkage for each structure are shown in Table I. Comparison of ϕ, ψ, and ω for the derestrained structure (III) with the restrained structure (II) indicates that the restrained minimized structure is energetically favorable, as expected due to the near equivalence

Table I: Values of ϕ, ψ, and ω for Each Glycosidic Linkage in the GPI Glycan for Each of Structures I–V

linkage[a]	min, I	restr min, II	derestr min, III	av restr, IV	av derestr, V
Glu–6Ino	−56.7[b]	−52.1	−52.9	−31.8	−37.5
2 1	−45.3[c]	−41.3	−41.8	−27.3	−30.4
Man–4Glu	−15.7	−16.8	−16.6	−10.4	−10.1
3 2	−28.1	−28.3	−28.1	−31.6	−28.2
Man–6Man*	3.4	2.1	1.2	−42.6	−41.8
4 3	170.4	171.4	171.3	−139.1	−176.5
	165.2[d]	165.2	165.3	157.3	174.7
Man–2Man	−41.5	−39.5	−39.3	−41.8	−43.3
5 4	4.3	3.1	3.2	−9.5	−9.9
Gal–3Man	−36.3	−36.5	−36.6	−44.2	−47.3
6 3	−23.2	−22.7	−22.8	−21.5	−26.5
Gal–6Gal*	−42.5	−43.7	−43.5	−12.1	−9.6
7 6	−96.3	−96.6	−96.7	−72.4	−72.6
	56.0	55.3	55.8	61.4	58.5
Gal–2Gal	−42.0	−40.6	−40.7	−35.1	−34.3
8 6	−26.4	−30.1	−29.9	−38.0	−38.0
Gal–2Gal	−32.1	−33.7	−33.2	−35.6	−34.5
9 7	−25.7	−27.9	−27.8	−33.8	−33.3

[a] An asterisk denotes the absence of NOE constraints about this linkage. [b] ϕ. [c] ψ. [d] ω.

Table II: Comparison of NOE-Derived Target Distances versus Restrained Minimum Distances Measured from Structure II

vector	target distance (Å)	restr min distance (Å)
$GlcNH_2$ H1–inositol H6	2.6	2.81
Man-1 H1–$GlcNH_2$ H4	2.4	2.28
Gal-4 H1–Man-1 H3	2.3	2.36
Gal-6 H1–Gal-4 H1	2.4	2.45
Gal-6 H1–Gal-4 H2	2.5	2.49
Gal-7 H1–Gal-5 H1	2.4	2.45
Gal-7 H1–Gal-5 H2	2.5	2.37
Man-2 H1–Man-3 H5	2.5	2.44
Man-3 H1–Man-2 H2	2.3	2.22

of structures I and II. In addition, the associated force constants for the NOE constraints are sufficient to constrain the relevant internuclear distances to values close to those measured experimentally (Table II). It should be noted that no NOE constraints were available for either the Manα1–6Man or the Galα1–6Gal linkages. The average values of ϕ, ψ, and ω in Cartesian space for each glycosidic linkage are generally similar between the restrained MD simulation (structure IV) and the derestrained MD simulation (structure V), indicating that the NOE restraints do not significantly perturb the dynamics trajectories. This is seen more clearly from a plot of rms deviation vs atom number (Figure 3, and Table III) for each simulation. The plots are in general quite similar, with the exception of the rms deviations for Man-3, which we attribute to a relatively poor curve fit for the potential surface of Manα1–2Man which was noted during the parametrization procedure. Attempts to improve this aspect of the parametrization are in progress.

A comparison between structures IV and II (or V or III) indicates that average values for ϕ and ψ are similar to their global minimum values for most linkages. Notable exceptions are ϕ and ψ for both Manα1–6Man and Galα1–6Gal and, to a lesser extent, ϕ and ψ for the glucosamine–inositol linkage. In these cases the average values are markedly different from the global minimum values. This cannot be attributed to the lack of NOE constraints in the case of the 1–6 linkages since the restrained (structure IV) and derestrained (V) average structures are similar. Rather, this in indicative of large torsional fluctuations about the α1–6 glycosidic linkages (which may explain the lack of measurable NOEs across these linkages), in a manner analogous to those described previously in oligomannose-type oligosaccharides (Homans et al., 1987c),

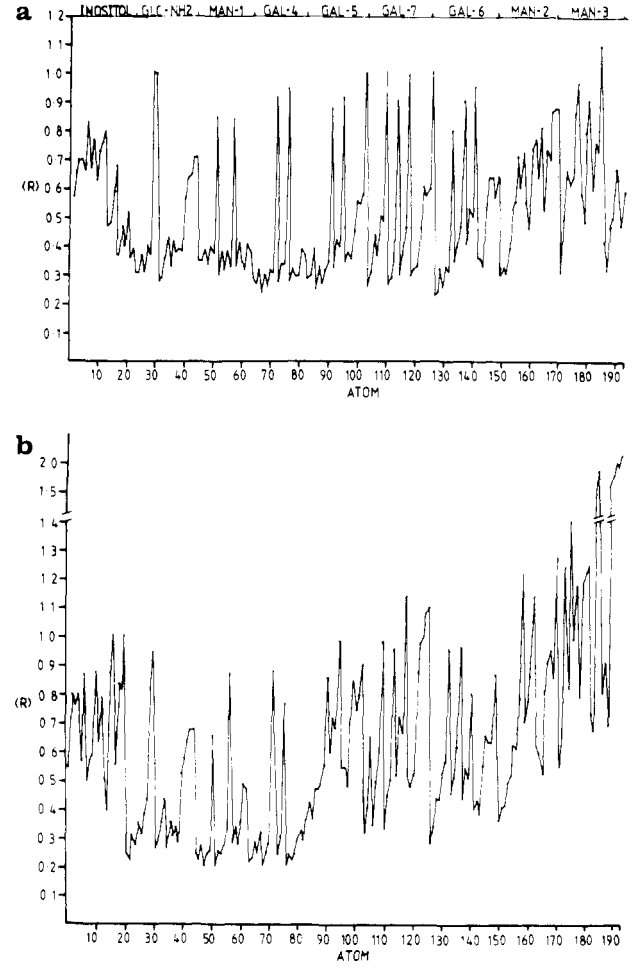

FIGURE 3: Plot of root mean square atomic fluctuations $R = (X^2 + Y^2 + Z^2)^{1/2}$ versus atom number (Table III) for the GPI glycan in (a) structure IV and (b) structure V.

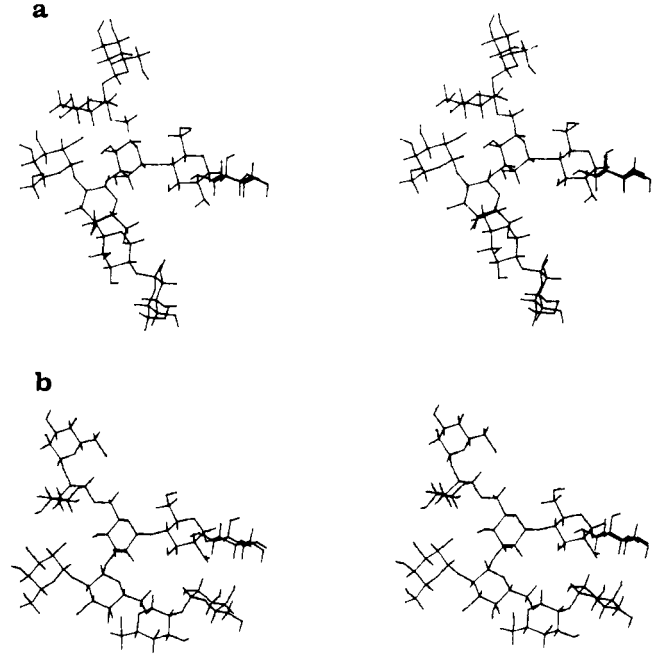

FIGURE 4: Stereoviews of (a) structure II and (b) structure V. In each case the inositol residue is at the right of the figure and the galactose side chain is at the lower left.

whereas for the majority of linkages, the torsional fluctations are small. The net effect of these differences is that the overall conformation represented by the average structures is different

Table III: Key to Atom Numbers Plotted in Figure 3[a]

residue no.	atom	residue no.	atom	residue no.	atom	residue no.	atom	residue no.	atom	residue no.	atom
		Inositol						Gal-7			
1	C1	9	C3	17	C5	104	O1	112	H3	120	H5
2	H1	10	H3	18	H5	105	C1	113	O3	121	OR
3	O1	11	O3	19	O5	106	H1	114	HO3	122	C6
4	HO1	12	HO3	20	HO5	107	C2	115	C4	123	H6A
k	C2	13	C4	21	C6	108	H2	116	H4	124	H6B
6	H2	14	H4	22	H6	109	O2	117	O4	125	O6
7	O2	15	O4	23	O6	110	HO2	118	HO4	126	HO6
8	HO2	16	HO4			111	C3	119	C5		
		Glucosamine						Gal-6			
24	C1	31	C3	39	OR	127	O1	135	H3	143	H5
25	H1	32	H3	40	C6	128	C1	136	O3	144	OR
26	C2	34	HO3	41	H6A	129	H1	137	HO3	145	C6
27	H2	35	C4	42	H6B	130	C2	138	C4	146	H6A
28	N1	36	H4	43	O6	131	H2	139	H4	147	H6B
29	HN1	37	C5	44	HO6	132	O2	140	O4	148	O6
30	HN2	38	H5			133	HO2	141	HO4	149	HO6
						134	C3	142	C5		
		Man-1									
45	O1	52	C3	58	C5			Man-2			
46	C1	53	H3	59	H5	150	O1	157	O3	164	H5
47	H1	54	C4	60	OR	151	C1	158	HO3	165	OR
48	C2	55	H4	61	C6	152	H1	159	C4	166	C6
49	H2	56	O4	62	H6A	153	C2	160	H4	167	H6A
50	O2	57	HO4	63	H6B	154	H2	161	O4	168	H6B
51	HO2					155	C3	162	HO4	169	O6
						156	H3	163	C5	170	HO6
		Gal-4									
64	O1	71	O3	77	C5			Man-3			
65	C1	72	HO3	78	H5	171	O1	179	H3	187	H5
66	H1	73	C4	79	OR	172	C1	180	O3	188	OR
67	C2	74	H4	80	C6	173	H1	181	HO3	189	C6
68	H2	75	O4	81	H6A	174	C2	182	C4	190	H6A
69	C3	76	HO4	82	H6B	175	H2	183	H4	191	H6B
70	H3					176	O2	184	O4	192	O6
						177	HO2	185	HO4	193	HO6
		Gal-5				178	C3	186	C5		
83	O1	90	O3	97	H5						
84	C1	91	HO3	98	OR						
85	H1	92	C4	99	C6						
86	C2	93	H4	100	H6A						
87	H2	94	O4	101	H6B						
88	C3	95	HO4	102	O6						
89	H3	96	C5	103	HO6						

[a] Carbon atoms are designated C and are labeled sequentially around the ring. Oxygen atoms, protons, and hydroxyl protons are labeled O, H, and HO, respectively, and the ring oxygen is designated OR.

from the global minimum conformation. This is illustrated in Figure 4 for the average derestrained structure (V) and the restrained minimized structure (II).

The values of ω for the Manα1–6Manα and Galα1–6Galα linkages remained essentially constant throughout the course of the MD simulation (Table I), and no averaging between rotamer populations (Homans et al., 1986) was observed on this time scale. This could not be investigated experimentally in the case of the Manα1–6Manα linkage since the values of $J_{5,6}$ and $J_{5,6'}$ for the 3,6-di-O-substituted mannose residue were obscured by extreme overlap of resonances in the COSY spectrum. In contrast, the values of $J_{5,6}$ and $J_{5,6'}$ were measurable for the 2,6-di-O-substituted galactose residue (3.1 ± 1.5 and 9.4 ± 1.5 Hz). Analysis of crystal structures (Marchessault & Perez, 1979) and NMR measurements on stereospecifically deuterated galactose derivatives (Bock & Refn, 1987; Ohrui et al., 1988) suggests that the $\omega = -60°$ and $\omega = +60°$ rotamers are preferred. In the absence of stereospecific assignments for H6 and H6′, the above coupling constants are consistent with either of these values. However, in the GPI anchor glycan, the $\omega = -60°$ rotamer would appear not to be populated significantly due to steric constraints imposed upon the galactose side chain in this conformation by the glucosamine–inositol moiety. However, the possibility of averaging between discrete rotamers on a time scale greater than that represented by the MD simulations cannot be excluded.

Discussion

From the results it is clear that the definition of a unique conformation for the GPI glycan is not possible. Apart from large torsional oscillations about α1–6 linkages, hydroxyl and free hydroxymethyl groups clearly undergo extreme torsional fluctuations on the picosecond time scale (Figure 3). The most suitable method by which a picture of this dynamic structure can be visualized is thus by display of the dynamics trajectories. The static structure shown in Figure 4b does, however, provide a perspective of the overall solution conformation. The structure exists in an extended configuration that spans a surface area of 600 Å^2. This is the same as the cross-sectional area of a monomeric N-terminal VSG domain (Metcalf et al., 1987), and the structure in situ might be considered to lie along the plane of the membrane, as shown in the hypothetical dimeric form in Figure 5. In this orientation the C-terminal and N-terminal domains of VSG lie above the glycan. Further, the attachments of the lipid and protein lie below and above the plane of the glycan, respectively. Thermodynamic assumptions indicate that the glycan does not penetrate the

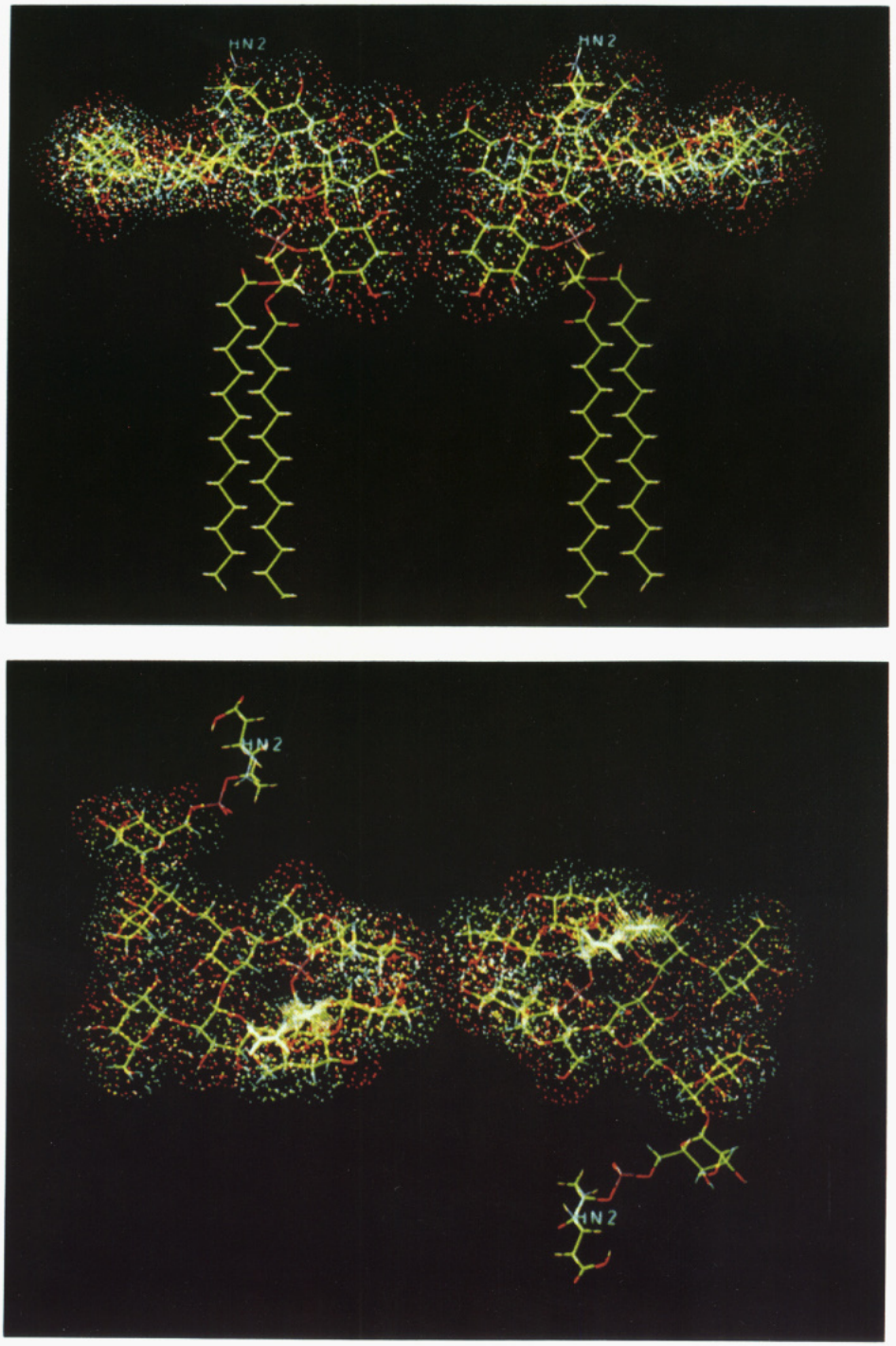

FIGURE 5: (Top) Diagrammatic representation of structure V with the addition of the fatty acyl chains, viewed along the plane of the membrane. The putative association of two GPI moieties in a VSG dimer is shown. The structure at the bottom shows a view which is perpendicular to that at the top. Each GPI spans an area of ~600 Å^2, which is the approximate cross-sectional area of the VSG N-terminal domain monomer. From this view it appears that the glycan lies along the plane of the membrane and the protein (attached at points HN2) lies above it. However, the precise orientation of the protein with respect to the glycan is not defined.

membrane. Clearly, this model represents a preliminary attempt to define the architecture of the VSG coat of MITat 1.4. A more sophisticated definition of the structure would involve performing the calculations in water and considering the possibility of hydrogen bonding between water and the glycan. Additionally, no account has been taken of possible interactions of the glycan with the protein or the constraints of association of the acyl chains with the lipid bilayer. Nevertheless, the overall volume occupied by the glycan (mol wt approximately 2000) is significant in comparison with the volume of the protein (mol wt approximately 55 000), and the orientation shown in Figure 5 maximizes the surface area presented to both membrane and protein. Taken together, these data provide a favorable argument for a space-filling role of the GPI glycan, which may be important in the dimerization of VSG molecules and/or the maintenance of the integrity of the VSG coat as a macromolecular diffusion barrier of different antigenic variants. In further support of this conclusion is the known correlation of the VSG C-terminal subgroup with glycan composition: group 1 VSGs contain three to four galactose residues, group 2 contain eight, and the one member of group 3 contains none. This suggests that the three-di-

mensional structure of the VSG C-terminal domain may modulate the accessibility of the anchor to the relevant α-galactosyltransferases. The latter might be considered as "spatial probes" that continue to extend the side chains until sterically prevented from doing so. This model is consistent with present knowledge regarding GPI transfer to protein. The VSG mRNA encodes short (17 or 23 amino acids) C-terminal peptide extensions, which serve as a signal for GPI addition and are rapidly removed and replaced by GPI in the rough endoplasmic reticulum (Bangs et al., 1985; Ferguson et al., 1986). Similar rapid kinetics have been observed for the transfer of GPI to thymocyte Thy-1 and mouse N-CAM_{120} (Conzelmann et al., 1987; He et al., 1987).

A putative GPI precursor species has been isolated from trypanosomes (Krakow et al., 1986; Menon et al., 1987), which contains dimyristylphosphatidylinositol, $GlcNH_2$, mannose, and ethanolamine but not galactose (Menon et al., 1987). The absence of galactose in this putative GPI precursor suggests that GPI galactosylation occurs after transfer to VSG polypeptide and could therefore be controlled by steric constraints imposed by the attached protein. An alternative possibility is that galactosylation is controlled by differential expression of transferases which might be encoded by the expression site associated genes in different variants (Van der Ploeg, 1987). However, this hypothesis is less likely since VSG MITat 1.4 (group 1) and VSG MITat 1.5 (group 3) appear to share the same expression site in the trypanosome genome (Van der Ploeg et al., 1982).

Regardless of the mechanism of galactosylation, a space-filling role for the galactose side chain is an important potential target for chemotherapy since inhibitors of the relevant α-galactosyltransferases might be trypanocidal through disruption of the integrity of the VSG coat and should have limited toxicity in the host since the presence of Galα1–2 in GPI appears to be parasite specific. In contrast, targets in the covalent backbone between the bridging ethanolamine phosphate and inositol phosphate may be less attractive, since structural studies on the Thy-1 anchor (Homans et al., 1988) suggest that the pathway for biosynthesis of this region of the molecule may be ubiquitous throughout the eukaryotes.

Acknowledgments

We acknowledge stimulating discussions with Prof. K. Bock and color photography by Jean Rotsaert.

Registry No. GPI glycan, 118920-09-5.

References

Bangs, J. D., Hereld, D., Krakow, J. L., Hart, G. W., & Englund, P. T. (1985) *Proc. Natl. Acad. Sci. U.S.A. 82*, 3207.

Bock, K., & Refn, S. (1987) *Acta Chem. Scand. B41*, 469.

Boothroyd, J. C. (1985) *Annu. Rev. Microbiol. 39*, 475.

Brisson, J.-R., & Carver, J. P. (1983a) *Biochemistry 22*, 1362.

Brisson, J.-R., & Carver, J. P. (1983b) *Biochemistry 22*, 3671.

Conzelmann, A., Spiazzi, A., & Bron, C. (1987) *Biochem. J. 246*, 605.

Cross, G. A. M. (1984) *Philos. Trans. R. Soc. London, B 307*, 3.

Cumming, D. A., & Carver, J. P. (1987) *Biochemistry 26*, 6664.

Dewar, M. J. S., & Stewart, J. J. P. (1986) *AMPAC, QCPE Bull.*, 506.

Ernst, R. R., Bodenhausen, G., & Wokaun, A. (1987) *Principles of NMR in one and two dimensions*, Clarendon Press, Oxford, and references cited therein.

Ferguson, M. A. J., & Williams, A. F. (1988) *Annu. Rev. Biochem. 57*, 285.

Ferguson, M. A. J., Duszenko, M., Lament, G. S., Overath, P., & Cross, G. A. M. (1986) *J. Biol. Chem. 261*, 356.

Ferguson, M. A. J., Homans, S. W., Dwek, R. A., & Rademacher, T. W. (1988) *Science 239*, 753.

He, H. T., Finne, J., & Gondis, C. (1987) *J. Cell Biol. 105*, 2489.

Homans, S. W., Dwek, R. A., Boyd, J., Mahmoudian, M., Richards, W. G., & Rademacher, T. W. (1986) *Biochemistry 25*, 6342.

Homans, S. W., Dwek, R. A., & Rademacher, T. W. (1987a) *Biochemistry 26*, 6571.

Homans, S. W., Dwek, R. A., & Rademacher, T. W. (1987b) *Biochemistry 26*, 6553.

Homans, S. W., Pastore, A., Dwek, R. A., & Rademacher, T. W. (1987c) *Biochemistry 26*, 6649.

Homans, S. W., Ferguson, M. A. J., Dwek, R. A., Rademacher, T. W., Anand, R., & Williams, A. F. (1988) *Nature 333*, 269.

Hopfinger, A. J., & Pearlstein, R. A. (1984) *J. Comput. Chem. 5*, 486.

Krakow, J. L., Hereld, D., Bangs, J. D., Hart, G. W., & Englund, P. T. (1986) *J. Biol. Chem. 261*, 12147.

Low, M. G., & Saltiel, A. R. (1988) *Cell 51*, 159.

Marchessault, R. H., & Perez, S. (1979) *Biopolymers 18*, 2369.

Menon, A. K., Mayor, S., Ferguson, M. A. J., Duszenko, M., & Cross, G. A. M. (1988) *J. Biol. Chem. 263*, 1970.

Metcalf, P., Blum, M., Freyman, D., Turner, M., & Wiley, D. C. (1987) *Nature 325*, 84.

Ohrui, H., Nishida, Y., Higuchi, H., Hon, H., & Meguro, H. (1987) *Can. J. Chem. 65*, 1145.

Paulsen, H., Peters, T., Sinnwell, V., Heume, M., & Meyer, B. (1986a) *Liebigs Ann. Chem. 5*, 951.

Paulsen, H., Peters, T., Sinnwell, V., Heume, M., & Meyer, B. (1986b) *Carbohydr. Res. 156*, 87.

Turner, M. J. (1985) *Br. Med. Bull. 41*, 137.

Van der Ploeg, L. H. (1987) *Cell 51*, 159.

Van der Ploeg, L. H., Bernards, A., Rijsewijk, F. A. M., & Borst, P. (1982) *Nucleic Acids Res. 10*, 593.

Weiner, S. J., Kollman, P., Nguyen, D. T., & Case, D. A. (1986) *J. Comput. Chem. 7*, 230.